Numerical study of solitary wave propagation in curved channels

Reprinted From Coastal Engineering 2000
Proceedings of the Conference
American Society of Civil Engineers
Held July 16-21, 2000, Sydney, Australia

Numerical Study of Solitary Wave Propagation in Curved Channels

Masatoshi Yuhi[1], Hajime Ishida[2] and Hajime Mase[3]

Abstract

A numerical model is developed for the extended Boussinesq equations expressed in the generalized curvilinear coordinate system. The model is applied to the study of solitary wave propagation through circular channels. The general features of solitary wave propagation are described and the effects of channel width and incident wave height on the transmission and reflection properties are examined. It is shown that the wave transformation becomes significant in wide channels. The maximum crest height at the outer wall of channel is then investigated in detail. The maximum crest height can reach almost twice as large as the incident wave amplitude in wide channels. The numerical results indicate that the maximum crest height can be correlated fairy well with a single dimensionless parameter.

1. Introduction

Physical understanding of the wave propagation in shallow water channels is essential for the accurate estimation of wave overtopping and the designing of effective counter-measures against it. From this point of view, extensive investigations have been carried out on the wave propagation in straight channels. On the contrary, relatively few studies can be found which treat the propagation of waves in curved channels. From engineering aspects, however, rivers, harbors and canals often have winding turns in direction. And therefore it is quite important to investigate how water waves propagate through curved channels.

Recently Shi et al. (1998) and Shi & Teng (1998) studied the characteristics of solitary wave propagation in sharp-cornered 90 degrees bends and in smoothly curved circular bends. In their study the transmitted and reflected wave height in relatively narrow channels were investigated. In this study we revisit the latter problem from a

1 Dept. Civil Eng., Kanazawa Univ., Kanazawa, 920-8667, Japan; yuhi@t.kanazawa-u.ac.jp
2 Dept. Civil Eng., Kanazawa Univ., Kanazawa, 920-8667, Japan;
3 Disaster Prevention Research Institute, Kyoto Univ., Uji, 611-0011, Japan;

different point of view toward the estimation of wave overtopping: Our focus is placed on the characteristics of the solitary wave propagation in wide circular channels. In particular the maximum crest height at the channel wall is examined in detail.

The objective of our study is twofold: At first, we aim to develop a reliable numerical model for long wave propagation in channels of arbitrary shape. And next, we intend to obtain the deep physical understanding and the practical engineering information on solitary wave propagation in wide circular channels. In particular we concentrate on the effects of channel geometry and the incident wave non-linearity on the maximum crest height at the outer channel wall. For these purposes, a numerical model based on the finite difference method is developed for the extended Boussinesq equations expressed in the generalized curvilinear coordinate system. The properties of transmission and reflection of a solitary wave are examined for circular channels of constant width and depth. The effects of channel width and incident wave height on maximum crest height at the outer wall of channel are investigated in detail. An attempt to correlate the maximum crest height with a dimensionless parameter is also made.

This paper is organized as follows. First the governing equations and the coordinate transformation are summarized in Section 2. In Section 3, we explain the method of numerical calculation. The numerical results for curved channels are shown and discussed in Section 4. Conclusions are summarized in Section 5.

2. Mathematical Formulation

2.1 Governing Equations

The extended Boussinesq equations (Nwogu 1993) are given in dimensionless form by

$$\frac{\partial \zeta}{\partial t}+\nabla\cdot[(h+\varepsilon\zeta)\mathbf{u}]+\mu^2\nabla\cdot\left[\left(\frac{z^2}{2}-\frac{h^2}{6}\right)h\nabla(\nabla\cdot\mathbf{u})\right]+\mu^2\nabla\cdot\left[\left(z+\frac{h}{2}\right)h\nabla(\nabla\cdot(h\mathbf{u}))\right]=0 \quad (1)$$

$$\frac{\partial \mathbf{u}}{\partial t}+\nabla\zeta+\varepsilon(\mathbf{u}\cdot\nabla)\mathbf{u}+\mu^2\left[\left(\frac{z^2}{2}\right)\nabla\left(\nabla\cdot\left(\frac{\partial \mathbf{u}}{\partial t}\right)\right)+z\nabla\left(\nabla\cdot\left(h\frac{\partial \mathbf{u}}{\partial t}\right)\right)\right]=0 \quad (2)$$

where ζ = surface elevation, h = local water depth, $\boldsymbol{u}=(u, v)$ = horizontal velocity at an arbitrary depth, z_α . Two dimensionless parameters, μ and ε, which represent the effects of dispersion and non-linearity, respectively, are defined as $\mu=h_0'/\lambda_0'$ and $\varepsilon=a_0'/\lambda_0'$, where h_0' is the representative water depth, λ_0' is the incident wavelength and a_0' is the incident wave amplitude, respectively. The primes denote dimensional quantities. For solitary waves, the effective wave length λ_e' is defined as the wavelength within which the surface elevation everywhere is larger than 1% of its amplitude. The definitions of the non-dimensional variables are the same as in Nwogu (1993).

These governing equations can be rearranged as

$$\frac{\partial \zeta}{\partial t}=E(\zeta,u,v) \quad \frac{\partial U}{\partial t}=F(\zeta,u,v) \quad \frac{\partial V}{\partial t}=G(\zeta,u,v) \quad (3)$$

where

$$U = u + \mu^2 h\left(b_1 h\frac{\partial^2 u}{\partial x^2} + b_2\frac{\partial^2 (hu)}{\partial x^2}\right),\quad V = v + \mu^2 h\left(b_1 h\frac{\partial^2 v}{\partial y^2} + b_2\frac{\partial^2 (hv)}{\partial y^2}\right) \tag{4}$$

are treated as simple variables in time-stepping procedure. The remaining terms, E, F, and G, are functions of ζ, u and v. These are defined as

$$E = -\frac{\partial}{\partial x}[(h+\varepsilon\zeta)u] - \frac{\partial}{\partial y}[(h+\varepsilon\zeta)v] - \mu^2\frac{\partial}{\partial x}\left[a_1 h^3\left(\frac{\partial^2 u}{\partial x^2} + \frac{\partial^2 v}{\partial x\partial y}\right) + a_2 h^2\left(\frac{\partial^2 hu}{\partial x^2} + \frac{\partial^2 hv}{\partial x\partial y}\right)\right]$$
$$- \mu^2\frac{\partial}{\partial y}\left[a_1 h^3\left(\frac{\partial^2 v}{\partial y^2} + \frac{\partial^2 u}{\partial x\partial y}\right) + a_2 h^2\left(\frac{\partial^2 hv}{\partial y^2} + \frac{\partial^2 hu}{\partial x\partial y}\right)\right] \tag{5}$$

$$F = -\frac{\partial\zeta}{\partial x} - \varepsilon\left(u\frac{\partial u}{\partial x} + v\frac{\partial u}{\partial y}\right) - \mu^2 h\frac{\partial}{\partial t}\left(b_1 h\frac{\partial^2 v}{\partial x\partial y} + b_2\frac{\partial^2 hv}{\partial x\partial y}\right) \tag{6}$$

$$G = -\frac{\partial\zeta}{\partial y} - \varepsilon\left(u\frac{\partial v}{\partial x} + v\frac{\partial v}{\partial y}\right) - \mu^2 h\frac{\partial}{\partial t}\left(b_1 h\frac{\partial^2 u}{\partial x\partial y} + b_2\frac{\partial^2 hu}{\partial x\partial y}\right) \tag{7}$$

The constants a_1, a_2, b_1, and b_2 are given by

$$a_1 = \frac{\beta^2}{2} - \frac{1}{6},\quad a_2 = \beta + \frac{1}{2},\quad b_1 = \frac{\beta^2}{2},\quad b_2 = \beta \tag{8}$$

where $\beta = z_\alpha/h$. The value of β was taken as -0.531 in this study.

2.2 Coordinate Transformation

Since the precise expression of the channel geometry is essentially important for the accurate calculation of wave propagation in curved channels, the following coordinate transformation is introduced to fit the numerical domain to the channel boundary:

$$x = x(\xi,\eta),\quad y = y(\xi,\eta) \tag{9}$$

where (x, y) are variables in physical plane and (ξ, η) are those in computational plane. According to the chain rule we can rewrite first order partial derivatives in the following way:

$$\frac{\partial}{\partial x} = a_{11}\frac{\partial}{\partial\xi} + a_{21}\frac{\partial}{\partial\eta},\qquad \frac{\partial}{\partial y} = a_{12}\frac{\partial}{\partial\xi} + a_{22}\frac{\partial}{\partial\eta} \tag{10}$$

where a_{ij} (i =1,2; j =1,2) are defined as

$$a_{11} = \frac{1}{J}\frac{\partial y}{\partial\eta},\ a_{21} = -\frac{1}{J}\frac{\partial y}{\partial\xi},\ a_{12} = -\frac{1}{J}\frac{\partial x}{\partial\eta},\ a_{22} = \frac{1}{J}\frac{\partial x}{\partial\xi} \tag{11}$$

and J denotes the Jacobian of the transformation

$$J = \frac{\partial x}{\partial\xi}\frac{\partial y}{\partial\eta} - \frac{\partial x}{\partial\eta}\frac{\partial y}{\partial\xi} \tag{12}$$

Applying these operators again to obtain second derivatives yields

$$\frac{\partial^2}{\partial x^2} = a_{11}{}^2 \frac{\partial^2}{\partial \xi^2} + 2a_{11}a_{21}\frac{\partial^2}{\partial \xi \partial \eta} + a_{21}{}^2 \frac{\partial^2}{\partial \eta^2} + b_{11}\frac{\partial}{\partial \xi} + b_{12}\frac{\partial}{\partial \eta} \tag{13a}$$

$$\frac{\partial^2}{\partial x \partial y} = a_{11}a_{12}\frac{\partial^2}{\partial \xi^2} + (a_{11}a_{22} + a_{21}a_{12})\frac{\partial^2}{\partial \xi \partial \eta} + a_{21}a_{22}\frac{\partial^2}{\partial \eta^2} + b_{21}\frac{\partial}{\partial \xi} + b_{22}\frac{\partial}{\partial \eta} \tag{13b}$$

$$\frac{\partial^2}{\partial y^2} = a_{12}{}^2 \frac{\partial^2}{\partial \xi^2} + 2a_{12}a_{22}\frac{\partial^2}{\partial \xi \partial \eta} + a_{22}{}^2 \frac{\partial^2}{\partial \eta^2} + b_{31}\frac{\partial}{\partial \xi} + b_{32}\frac{\partial}{\partial \eta} \tag{13c}$$

where b_{ij} (i =1,3; j =1,2) are given by

$$\left.\begin{aligned} b_{11} &= -a_{12}c_{11} - a_{11}c_{12}, \quad b_{12} = -a_{22}c_{11} - a_{21}c_{12} \\ b_{21} &= c_{21}/J, \qquad\qquad b_{22} = c_{22}/J \\ b_{31} &= -a_{12}c_{31} - a_{11}c_{32}, \quad b_{32} = -a_{22}c_{31} - a_{21}c_{32} \end{aligned}\right\} \tag{14}$$

and

$$\left.\begin{aligned} c_{11} &= a_{11}{}^2 \frac{\partial^2 y}{\partial \xi^2} + 2a_{11}a_{21}\frac{\partial^2 y}{\partial \xi \partial \eta} + a_{21}{}^2 \frac{\partial^2 y}{\partial \eta^2} \\ c_{12} &= a_{11}{}^2 \frac{\partial^2 x}{\partial \xi^2} + 2a_{11}a_{21}\frac{\partial^2 x}{\partial \xi \partial \eta} + a_{21}{}^2 \frac{\partial^2 x}{\partial \eta^2} \\ c_{21} &= a_{22}\frac{\partial^2 y}{\partial \eta^2} + a_{12}\frac{\partial^2 y}{\partial \xi \partial \eta} - a_{11}a_{12}\frac{\partial J}{\partial \xi} - a_{11}a_{22}\frac{\partial J}{\partial \eta} \\ c_{22} &= -a_{12}\frac{\partial^2 y}{\partial \xi^2} - a_{22}\frac{\partial^2 y}{\partial \xi \partial \eta} - a_{21}a_{12}\frac{\partial J}{\partial \xi} - a_{21}a_{22}\frac{\partial J}{\partial \eta} \\ c_{31} &= a_{12}{}^2 \frac{\partial^2 y}{\partial \xi^2} + 2a_{12}a_{22}\frac{\partial^2 y}{\partial \xi \partial \eta} + a_{22}{}^2 \frac{\partial^2 y}{\partial \eta^2} \\ c_{32} &= a_{12}{}^2 \frac{\partial^2 x}{\partial \xi^2} + 2a_{12}a_{22}\frac{\partial^2 x}{\partial \xi \partial \eta} + a_{22}{}^2 \frac{\partial^2 x}{\partial \eta^2} \end{aligned}\right\} \tag{15}$$

In principle it is possible to apply the operators once again to obtain the analytical expression for the third spatial derivatives. However, the resulting expression becomes quite complicated and the metric tensor involved in the formulae requires very large computer memory. We therefore chose to calculate the third derivatives through a two-step procedure. Namely when we calculate the third derivative of a function *f*, we first evaluate the second derivative of *f* numerically and then differentiate it once again numerically to obtain the value of the third derivative. The accuracy of this procedure has been confirmed through several tests.

3. Numerical Model

Wei and Kirby(1995) developed a high-order numerical scheme for the extended Boussinesq equations in Cartesian coordinates. In this study, we slightly modified their numerical method and extend it for the generalized curvilinear coordinate system.

A fourth-order predictor-corrector scheme is adopted for time-stepping procedure. The predictor step is the third-order Adams-Bashforth scheme (Press et al. 1989) :

$$\zeta_{i,j}^{n+1^*} = \zeta_{i,j}^{n} + \frac{\Delta t}{12}\left(23E_{i,j}^{n} - 16E_{i,j}^{n-1} + 5E_{i,j}^{n-2}\right) \tag{16a}$$

$$U_{i,j}^{n+1^*} = U_{i,j}^{n} + \frac{\Delta t}{12}\left(23F_{i,j}^{n} - 16F_{i,j}^{n-1} + 5F_{i,j}^{n-2}\right) \tag{16b}$$

$$V_{i,j}^{n+1^*} = V_{i,j}^{n} + \frac{\Delta t}{12}\left(23G_{i,j}^{n} - 16G_{i,j}^{n-1} + 5G_{i,j}^{n-2}\right) \tag{16c}$$

where all information on the right hand side is known from previous calculations. The predictor values of horizontal velocities, $u_{i,j}^{n+1*}$ and $v_{i,j}^{n+1*}$, can then be obtained by solving Eq.(4) numerically in the generalized coordinate system. From the predicted values of surface elevation and horizontal velocities, the corresponding values of E, F, and G are calculated. The corrector scheme is the fourth-order implicit Adams-Moulton method, which is given by

$$\zeta_{i,j}^{n+1} = \zeta_{i,j}^{n} + \frac{\Delta t}{24}\left(9E_{i,j}^{n+1^*} + 19E_{i,j}^{n} - 5E_{i,j}^{n-1} + E_{i,j}^{n-2}\right) \tag{17a}$$

$$U_{i,j}^{n+1} = U_{i,j}^{n} + \frac{\Delta t}{24}\left(9F_{i,j}^{n+1^*} + 19F_{i,j}^{n} - 5F_{i,j}^{n-1} + F_{i,j}^{n-2}\right) \tag{17b}$$

$$V_{i,j}^{n+1} = V_{i,j}^{n} + \frac{\Delta t}{24}\left(9G_{i,j}^{n+1^*} + 19G_{i,j}^{n} - 5G_{i,j}^{n-1} + G_{i,j}^{n-2}\right) \tag{17c}$$

The corrector step is iterated until the error between two successive iterations reduces below a required criterion. The error is defined as

$$\Delta f = \frac{\sum_{i,j}\left|f_{i,j}^{n+1} - f_{i,j}^{n+1^*}\right|}{\sum_{i,j}\left|f_{i,j}^{n+1}\right|} \tag{18}$$

in which f represents each of the three dependent variables, ζ, u, v, and ()* denotes the previous estimate. The corrector step is iterated if any of the value of Δf exceeds 0.0001. Then the same procedure is applied to the next time step.

For first-order spatial derivatives, we adopt the fourth-order central difference. On the other hand, second-order spatial derivatives are approximated by second-order central differences. All the equations are discretized on an unstaggered grid.

In order to examine the accuracy of the numerical scheme, we calculated the propagation of a solitary wave in a straight channel of constant depth (h_0') and width. The total length of the channel is set to be 100 h_0' and the channel width is set to be 5 h_0'. A solitary wave is generated at the left boundary according to the analytical solution of Wei & Kirby (1995). The wave is transmitted at the right boundary. The corresponding values of ε and μ are 0.3 and 0.071, respectively.

The spatial profiles of the solitary wave on the center-plane of the channel are described in Fig.1 for various time instants. The initial waveform undergoes small evolution, which results in a slightly (about 3%) larger wave height. This is partially because the analytical solution used at the incident boundary is only asymptotically equivalent to the numerical model. In figure 2, solitary wave profiles are compared at two widely separated instances in time. The two waveforms are translated by an amount predicted by the analytical phase speed. The results show that the wave propagates for a long distance (at least 50 water depths) without any distortion except for the initial small evolution. The error in phase celerity was found to be less than 0.6%. The total mass is almost completely (more than 99.9%) conserved. These results thus validate the reasonably high accuracy of the numerical scheme.

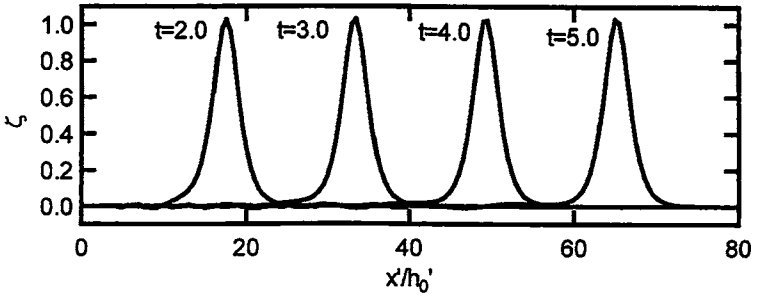

Figure 1. Spatial profiles of solitary wave in an straight channel at various time instants

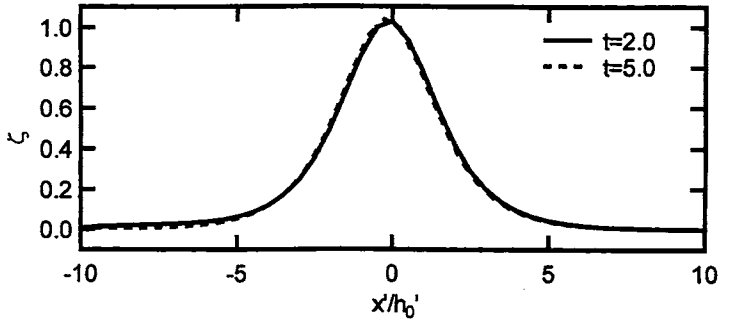

Figure 2. Comparison of solitary wave shapes at $t = 2.0$ and $t = 5.0$

4. Solitary Wave Propagation in Circular Channels

The geometry of the curved channel is shown in Fig.3 schematically. The channel is composed of a circular bend plus upstream and downstream legs. The water depth h_0' and the channel width W' are constant throughout the channel. The inner radius of the circular corner is 10 times as large as the water depth. The upstream and downstream legs are 50 times as long as the water depth. The inner and outer walls are vertical.

At the incident boundary, we specify the entire signal of ζ and $\boldsymbol{u}$ from the analytical solution of the extended Boussinesq equations (Wei & Kirby 1995). The radiation condition combined with wave damping layer is used at the transmitting boundary. At the inner and outer walls, the approximate conditions for general reflective boundaries with outward normal vector $\boldsymbol{n}$ (Wei & Kirby 1995) are imposed

$$\mathbf{u}\cdot\mathbf{n}=0, \quad \nabla\zeta\cdot\mathbf{n}=0, \quad \frac{\partial u_T}{\partial n}=0 \tag{19}$$

in which u_T is the velocity component tangent to the wall.

In the following, the effects of relative channel width, W'/h_0', and the incident wave nolinearity, $\varepsilon=a_0'/h_0'$, on the solitary wave propagation are investigated in detail. Calculations are carried out for $W'/h_0' = 5$, 10, 20 and ε from 0.05 to 0.30.

4.1 General Features of Transmission and Reflection

The numerical results for a solitary wave of small non-linearity (ε=0.05) through a narrow channel (W'/h_0'= 5) are shown in Fig.4 (a)-(e). These figures show the evolution of the free surface at various time instants through the circular bend. When the incident wave arrives at the curved section, the wave is nearly one-dimensional and the

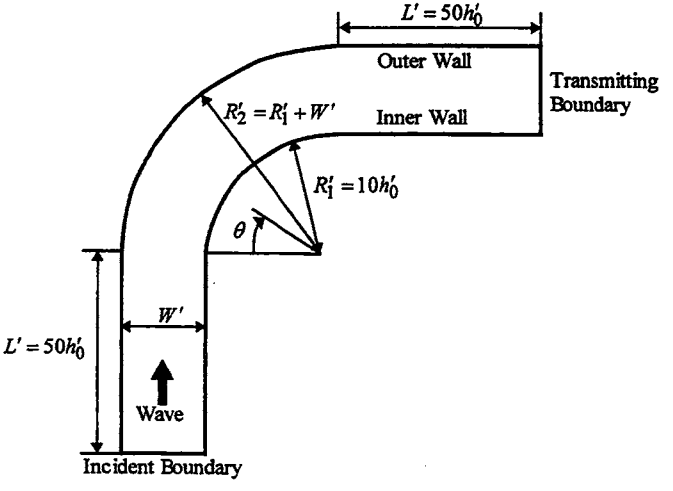

Figure 3. Geometry of the curved channel

initial wave profile is almost completely preserved. During its passage through the bend, however, the wave tilts higher outward against the outer wall. The difference of wave height in radial direction keeps balance with the centrifugal force. In such a case, the wave propagates faster in outer region, because the phase speed of the solitary wave increases with wave height. The increase of phase speed balances with the increase of the propagation length along the wall in outer region, which result in radially straight crest line. After passing through the bend, the wave recovers its initial shape quickly to make the wave crest uniform across the channel. It is seen from these results that the solitary wave is almost completely transmitted with little reflection in narrow circular channels. These results are consistent with the works by Shi et al.(1995).

The numerical results for the solitary wave of non-linearity $\varepsilon = 0.15$ through a channel with moderate width ($W'/h_0' = 10$) are shown in Fig.5(a)-(e). Just after the solitary wave enters into the circular part, the wave tilts higher outward against the outer wall. This shape is similar to the one recognized in the narrow channel results. However, during its passage through the bend, the characteristics of wave transformation are quite different. The solitary wave becomes no longer radially straight and the transmitted wave loses its initial shape. The amplification of the crest height is significant around the middle of the circular part.

Numerical results for the solitary wave of a large wave height ($\varepsilon = 0.25$) through a wide channel ($W'/h_0' = 20$) are shown in Fig.6(a)-(e). The main features seen in the case of moderate width are enhanced and the properties of transmission and reflection are quite different from those in the narrow channel. As the wave propagates through the circular bend, the wave tends to diffract near inner wall. The wave height of diffracted wave decreases gradually as it travels. On the other hand, the wave tends to travel straight near the outer wall. The crest height increases as the wave travels through the channel. The maximum crest height is attained around the middle of the outer wall and then the wave is reflected into inner region. The maximum crest height at the outer wall reaches almost 200% of the incident wave amplitude in this case. After the wave passed through the bend, the reflected wave propagates toward the inner wall. As a result, the wave height at the inner wall becomes higher, in turn. The maximum wave height at the inner wall is, however, much smaller than that attained at the outer wall. Since the reflected wave propagates much faster along the wall than the diffracted wave, the former catches up with the latter to merge into one wave in the final stage. From the comparison between the narrow and wide channel results, it is found that the amplitude of the transmitted wave decreases as the channel width increases.

When waves incident to a straight wall with small incident angle, the regular type of reflection gives way to another type of reflection, which is called 'Mach reflection' (e.g. Tanaka 1993). In Mach reflection, three kinds of waves are present near the wall: the incident wave, the reflected wave and a wave propagating along the wall called the stem wave. The wave height of stem wave can grow significantly along the wall. In the winding part of curved channels, waves incident to the outer wall with small angle, and therefore we may expect that the same situation arises as mentioned above. The situation in curved channels is, however, more complicated because the wall is not straight and the incident angle increases gradually as the wave propagates. According to the previous works on the Mach reflection along a straight wall, the development of

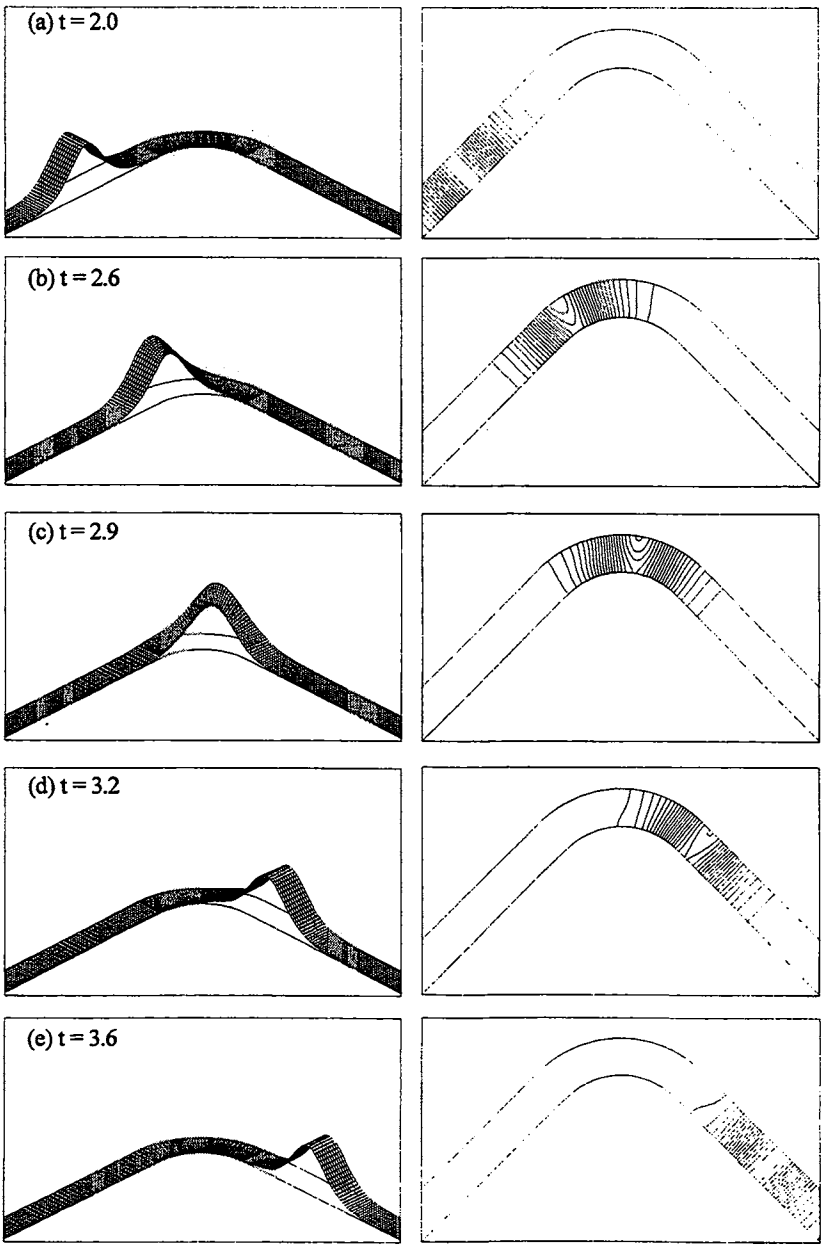

Figure 4. 3D and contour plots of the free surface elevation ($\varepsilon = 0.05$, $W'/h_0' = 5$)

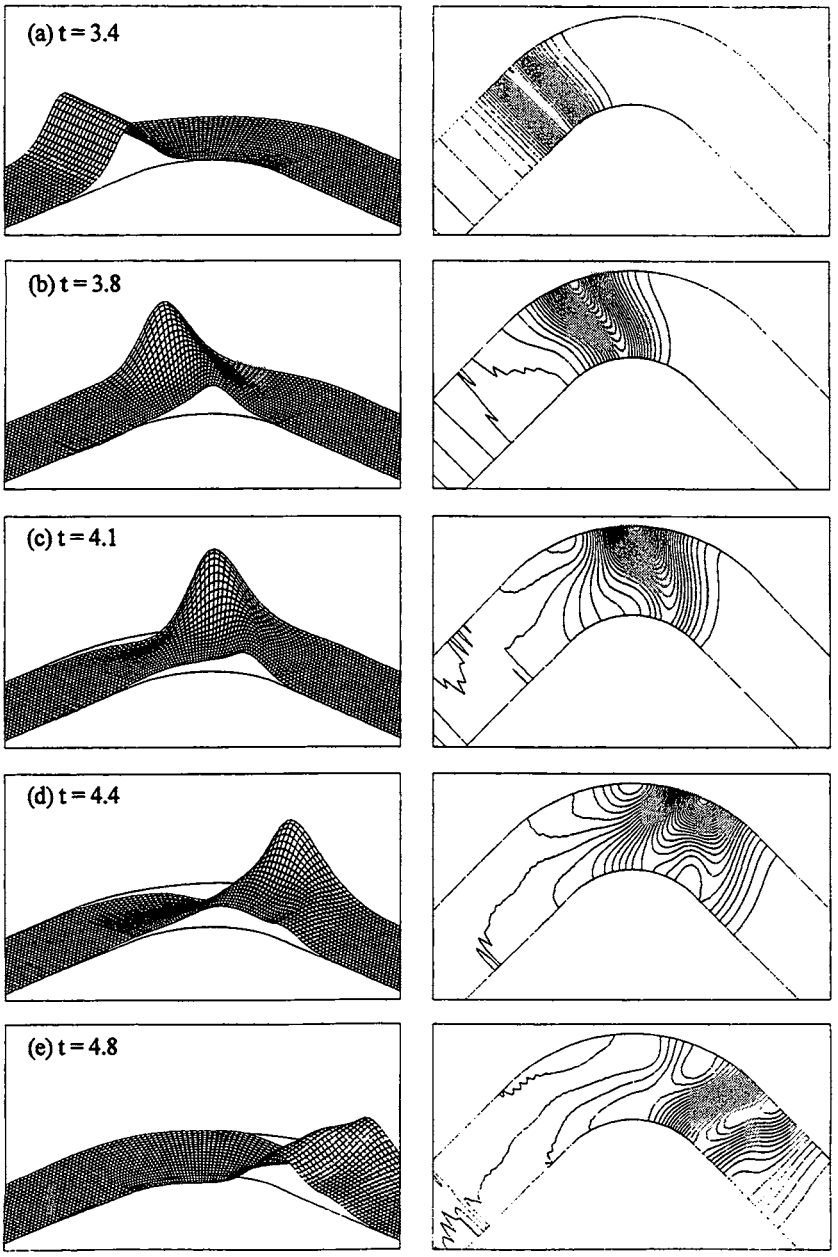

Figure 5. 3D and contour plots of the free surface elevation ($\varepsilon = 0.15$, $W'/h_0' = 10$)

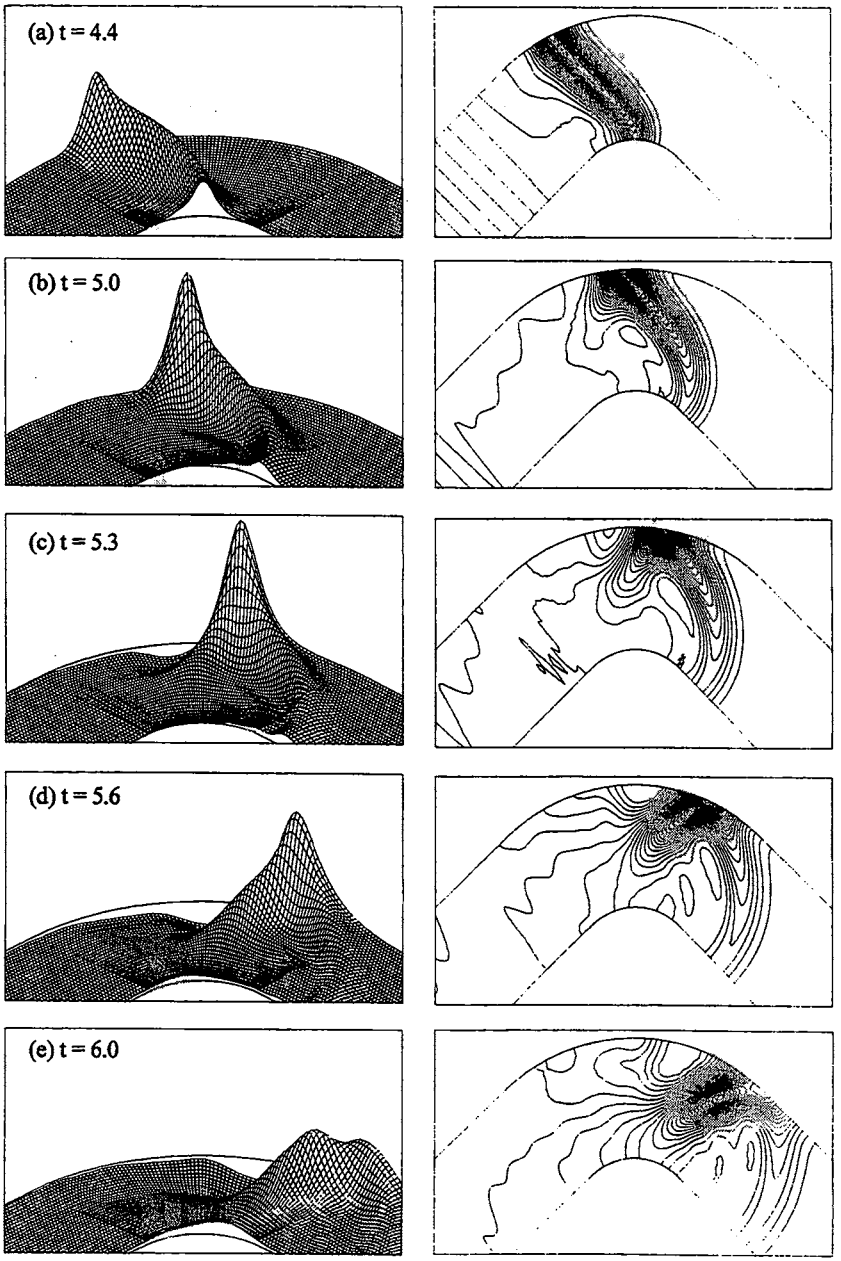

Figure 6. 3D and contour plots of the free surface elevation ($\varepsilon = 0.25$, $W'/h_0' = 20$)

stem wave is limited to the case of small incident angle. Hence, the gradual increase of the incident angle may prevent the development of the stem wave. In addition, Mach reflection is quite a slow phenomenon and therefore it takes very long time and distance for the stem wave to be fully developed. For these reasons, it is probable that the Mach reflection can be seen only in the channel with very mildly curved walls. The wave patterns shown in Fig.6(c) and (d) are similar to the ones in Mach reflection at the straight wall, but it cannot be decided, at present, whether this may be called a Mach reflection or not. Further investigations are necessary for precise discussion.

4.2 Maximum Crest Height at the Outer Wall

It is very important to predict the maximum crest height at channel walls in order to estimate the wave overtopping from channels. In Fig.7, the maximum crest height normalized by the incident wave amplitude ($\zeta_{max}=\zeta'/a_0'$) is plotted as a function of ε for various values of relative channel width. As ε increases, the crest height gradually increases and asymptotes to a constant value for each case. It is also seen that the maximum height is an increasing function of the relative channel width. We also investigated the angular location, θ_{max}, at which the maximum crest height is attained. The angle θ is taken clockwise as shown in Fig.3. The results are shown in Fig.8. In the case of the narrow channel, the position gradually moves downstream as ε increases. For wider channels, however, the location is insensitive to ε and takes almost the constant value of 48 and 53 degrees, respectively. In general, the location moves to the downstream direction as the channel width increases.

Finally an attempt to correlate the maximum crest height with a dimensionless parameter is made. In figure 9 the maximum crest height is plotted against the dimensionless parameter α which is defined as:

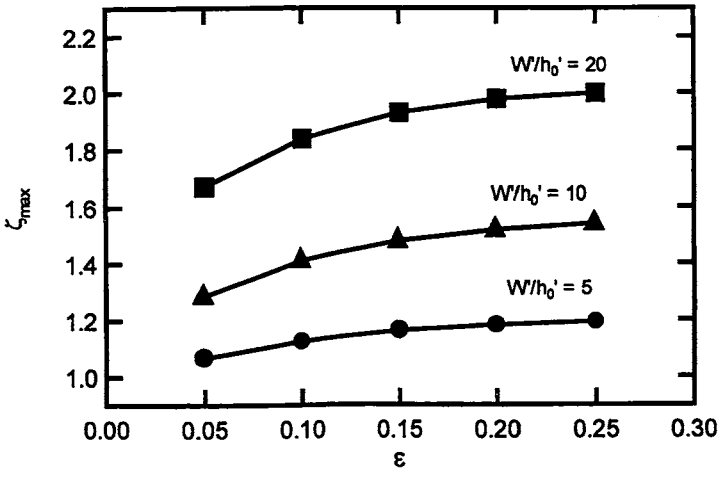

Figure 7. Maximum crest height at the outer wall of channel

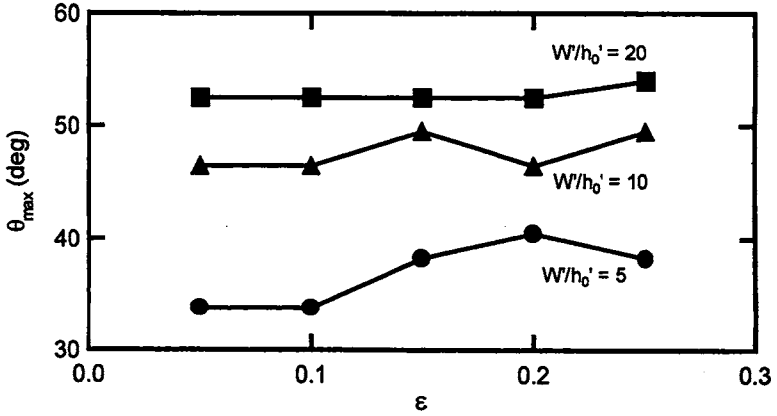

Figure 8. The angular location where the maximum crest height is attained

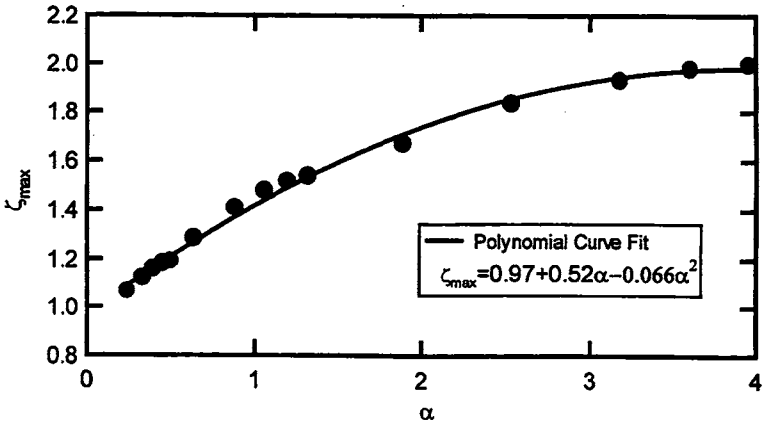

Figure 9. Maximum crest height against the dimensionless parameter α

$$\alpha = \frac{W'}{\lambda_e'} \times \frac{R_2'}{R_1'} \tag{20}$$

in which R_1' and R_2' represent the inner and outer radius of the circular part, respectively. The result is correlated fairly well by this parameter. On the basis of the numerical results presented in Fig.9, an empirical formula for predicting the maximum crest height at the outer wall is obtained as follows:

$$\zeta_{max} = 0.97 + 0.52\alpha - 0.066\alpha^2 \tag{21}$$

In our computations, the typical values of the dimensionless grid sizes used for Δx,

Δy, and Δt in the physical plane are 0.025, 0.025 and 0.015, respectively. Several calculations have been carried out on a different grid spacing as $\Delta x \equiv \Delta y \equiv 0.017$ and $\Delta t = 0.01$. Almost the same results are obtained. The relative difference of the maximum crest height is about 1%. The conservation of total mass has also been checked. The error in total mass was about 2%.

5. Conclusions

A high order numerical scheme was developed for the extended Boussinesq equations expressed in the generalized curvilinear coordinate system. By applying it to the problem of solitary wave propagation through circular channels, the following results were obtained.

When a solitary wave propagates through a narrow circular channel, the wave is transmitted almost completely with little reflection. The shape of the transmitted wave is almost the same as that of the incident wave. This is consistent with the results for long wave propagation in a narrow curved channel by Shi et al. (1998). For a solitary wave traveling through a wide channel, the wave transformation is significant. In this case, the transmitted wave no longer preserves its original shape and disintegrates into several smaller waves. This is due to the combined effects of the diffraction at the corner and the lateral reflection from the channel wall.

The maximum surface elevation at the outer channel wall can reach almost 200% of the incident wave amplitude for wide channels. These values can be predicted fairly well with one dimensionless parameter.

Finally, we mention that the numerical model developed in this study is applicable to the channels with more generalized geometry and bottom topography. Furthermore the extension to branching channels is not a difficult task. The treatments of regular and irregular waves can also be made straightforwardly. Further numerical investigations are being planned.

References

Nwogu, O. (1993) : Alternative form of Boussinesq equations for nearshore wave propagation, *J.Wtrwy., Port, Coast. and Oc. Engrg.*, Vol. 119, No.6, pp.618-638.

Press, W.H., Flannery, B.P., Teukolsky, S.A. and Vetterling, W.T. (1989) : *Numerical Recipes*, Cambridge University Press, Neo York, pp.569-572.

Shi, A. , Teng, M.H. and Wu, T. (1998): Propagation of solitary waves through significantly curved shallow water channels, *J. Fluid Mech.*, Vol.362, pp.157-176.

Shi, A. ,and Teng, M.H. (1998): Linear and nonlinear modeling of long waves propagating around channel bends, *Proc. 26th Int. Conf. Coastal Eng., ASCE*, pp.433-442.

Tanaka, M. (1993) : Mach reflection of a large-amplitude solitary wave, *J. Fluid Mech.*, Vol.248, pp.637-661.

Wei, G. and Kirby, J.T. (1995): Time-dependent numerical code for extended Boussinesq equations, *J.Wtrwy., Port, Coast., and Oc. Engrg.*, Vol. 121, No.5, pp.251-261.